Published OnlineFirst December 17, 2012; DOI: 10.1158/0008-5472.CAN-12-1979

Application of a Proapoptotic Peptide to Intratumorally Spreading Cancer Therapy

Renwei Chen[1,2], Gary B. Braun[1,2], Xiuquan Luo[1,2], Kazuki N. Sugahara[1,2], Tambet Teesalu[1,2], and Erkki Ruoslahti[1,2]

Abstract

Bit1 is a proapoptotic mitochondrial protein associated with anoikis. Upon cell detachment, Bit1 is released into the cytoplasm and triggers caspase-independent cell death. Bit1 consists of 179 amino acids; for the C-terminal, two thirds of the molecule functions as a peptidyl-tRNA hydrolase, whereas the N-terminus contains a mitochondrial localization signal. Here, we localize the cell death domain (CDD) to the N-terminal 62 amino acids of Bit1 by transfecting cells with truncated Bit1 cDNA constructs. CDD was more potent in killing cells than the full-length Bit1 protein when equivalent amounts of cDNA were transfected. To develop Bit1 CDD into a cancer therapeutic, we engineered a recombinant protein consisting of the CDD fused to iRGD, which is a tumor-specific peptide with unique tumor-penetrating and cell-internalizing properties. iRGD-CDD internalized into cultured tumor cells through a neuropilin-1–activated pathway and triggered cell death. Importantly, iRGD-CDD spread extensively within the tumor when injected intratumorally into orthotopically implanted breast tumors in mice. Repeated treatment with iRGD-CDD strongly inhibited tumor growth, resulting in an average reduction of 77% in tumor volume and eradication of some tumors. The caspase independence of Bit1-induced cell death makes CDD a potentially attractive anticancer agent, because tumor resistance to the main mechanisms of apoptosis is circumvented. Using iRGD to facilitate the spreading of a therapeutic agent throughout the tumor mass may be a useful adjunct to local therapy for tumors that are surgically inoperable or difficult to treat systemically. *Cancer Res; 73(4); 1352–61. ©2012 AACR.*

Introduction

Cell–matrix interactions are important for cell survival and failure of cells to adhere to the extracellular matrix results in anoikis (1). Bit1 is a mitochondrial peptidyl-tRNA hydrolase that causes cell death when released into the cytoplasm or experimentally expressed there (2). Bit1 release occurs upon loss of cell attachment, resulting in cell death (2). Bit1 negatively regulates extracellular signal–regulated kinase (Erk) activation, revealing a possible molecular pathway for the anoikis regulation (3, 4). Cytosolic Bit1 interacts with the Groucho family transcriptional coregulator amino-terminal enhancer of split (AES) to induce caspase-independent cell death (2). These activities and the ability of Bit1 to counteract transducin-like enhancer of split 1 (TLE1), which is an antiapoptotic oncoprotein, suggest a tumor suppressor role for Bit1 (2, 5, 6). A unique property of Bit1 is that cell attachment through certain integrins can prevent cell death induced by cytoplasmic Bit1, whereas various antiapoptotic signaling molecules, such as Bcl-2, Bcl-xL, PI-3K, and Akt, can prevent the release of Bit1 from mitochondria but are unable to rescue the cell death caused by cytoplasmic Bit1 (2).

Bit1 is a 179-amino acid protein in which amino acids 63 to 179 at the C-terminus of the molecule constitute the catalytic, peptidyl-tRNA hydrolase 2 (Pth2) domain, and the N-terminus serves as a mitochondrial localization signal (2, 7). It is also known that the N-terminal domain is needed for the apoptotic activity (2, 7), but the active site has not been mapped in detail and the mechanism whereby Bit1 causes cell death is not fully understood. We undertook this study to define the cell death domain (CDD) of Bit1, delineate its mechanism of action, and explore its use as an antitumor drug. To deliver Bit1 CDD protein into tumor cells and deal with the problem of poor penetration of anticancer drugs in solid tumors (8, 9), we used so-called C-end Rule or CendR peptides. These peptides contain a CendR motif (R/KXXR/K), which binds to neuropilin-1 (NRP-1) triggering a cell internalization and tissue penetration pathway (10, 11). The CendR motif has to be at the C-terminus of the peptide to be active. The iRGD peptide contains a cryptic CendR motif (sequence: CRGDKGPDC; CendR motif underlined). This peptide activates the CendR pathway specifically in tumors because it first binds to αvβ3 and αvβ5 integrins, which

Authors' Affiliations: [1]Center for Nanomedicine, Sanford-Burnham Medical Research Institute, University of California, Santa Barbara, Santa Barbara; and [2]Cancer Research Center, Sanford-Burnham Medical Research Institute, La Jolla, California

Note: Supplementary data for this article are available at Cancer Research Online (http://cancerres.aacrjournals.org/).

Current address for X. Luo: University of Texas Southwestern Medical Center, Simmons Comprehensive Cancer Center, Dallas, TX.

Corresponding Author: Erkki Ruoslahti, Sanford-Burnham Medical Research Institute, 10901 North Torrey Pines Rd., La Jolla, CA 92037. Phone: 858-795-5023; Fax: 858-795-5323; E-mail: ruoslahti@sanfordburnham.org

doi: 10.1158/0008-5472.CAN-12-1979

Published OnlineFirst December 17, 2012; DOI: 10.1158/0008-5472.CAN-12-1979

are expressed in tumor vessels and various types of other cells within tumors but not in normal tissues. Having bound to the integrins in a tumor, iRGD is proteolytically cleaved to generate a fragment with a C-terminal CendR motif that binds to NRP-1 and activates the CendR pathway (10).

Materials and Methods

Reagents, cell lines, and tumors

Mouse anti-human NRP-1 monoclonal antibody was purchased from Miltenyi Biotec Inc; rabbit anti-Ki-67 polyclonal antibody was from Abcam; mouse anti-β-actin monoclonal antibody was from Sigma-Aldrich; the secondary antibodies used were Alexa Fluor 488-conjugated goat immunoglobulin G (IgG; Invitrogen Life Technologies). Full-length cDNA for Bit1 in the mammalian expression vector pCMV-myc were generated previously in the laboratory (2). QuikChange Mutagenesis Kit for Bit1 mutagenesis was purchased from Agilent Technologies. In Situ Cell Death Detection Kit for terminal deoxynucleotidyl transferase–mediated dUTP nick end labeling (TUNEL) and FuGENE6 Transfection Reagent for overexpression was purchased from Roche Applied Science. MTT for cell viability assay was from Invitrogen Life Technologies.

Cell lines of human embryonic kidney (HEK) 293T, prostate cancer PPC1, and mouse breast cancer 4T1 were purchased from American Type Culture Collection (ATCC). Human tumor cell line M21 was a gift from Dr. David Cheresh at University of California, San Diego (San Diego, CA). Human breast cancer cell line MCF-10CA1a was obtained from the Barbara Ann Karmanos Cancer Institute (Detroit, MI). All the human cell lines were maintained in Dulbecco's Modified Eagle's Medium (DMEM) with glutamine containing 10% FBS, penicillin, and streptomycin at 37°C and 5% CO_2. The mouse 4T1 cell line was maintained in Iscove's Modified Dulbecco's Medium with glutamine containing 10% FBS, penicillin, and streptomycin. The HEK 293T and 4T1 cells were recently purchased from the ATCC and did not require further authentication. Seventeen short tandem repeat (STR) profiling by ATCC Cell Authentication Service authenticated the MCF-10CA1a and PPC1 (PC3) cells lines. The M21 showed similarity to the HTB-129 (MDA-MB-435S) line in this analysis. The origin of these cells is not critical for our purposes because we only used these cells to represent NRP-1-deficient, αv integrin-positive cells.

To produce orthotopic tumors, 1 million of tumor cells in 100 μL of PBS were injected into the mammary fat pad of mice. Athymic nude mice (Harlan Laboratories) were used for MCF-10CA1a cells and normal Balb/C mice (Charles River) for 4T1 cells. All animal procedures were carried out in compliance with the guidelines approved by the Animal Research Committee at the University of California, Santa Barbara (Santa Barbara, CA).

Construction and production of recombinant CDD proteins

Recombinant CDD proteins were prepared as follows: the CDD sequence was cloned into the bacterial expression vector pRSET containing a hexahistidine tag (Invitrogen Life Technologies). Because CDD harbors a mitochondrial signal peptide, a myc-tag was placed at the N-terminus of CDD to prevent the fusion protein from localizing to mitochondria. To generate cell- and tissue-penetrating CDD proteins, oligonucleotides encoding the CendR peptides, RPARPAR (11) or iRGD (sequence: CRGDKGPDC; ref. 10) were synthesized and ligated to the downstream of oligonucleotides encoding the CDD, with a glycine–serine linker placed in between (Supplementary Fig. S1A). All construct sequences were confirmed by DNA sequencing. Proteins were expressed in *Escherichia coli* BL21 (DE3) plysS strain (Novagen) after induction at 30°C for 24 hours using MagicMedia *E. coli* Expression Medium (Invitrogen Life Technologies) according to the manufacturer's instructions. The recombinant proteins were purified using nickel-nitrilotriacetic acid affinity chromatography under native conditions by using ÄKTA fast protein liquid chromatography system. The bound proteins were eluted with 20 mmol/L sodium phosphate buffer containing 300 mmol/L imidazole, pH 8.0. The eluates were dialyzed against PBS pH 7.4 containing an additional 360 mmol/L NaCl. In some experiments, the his-tag was removed using enterokinase (Invitrogen Life Technologies) according to the manufacturer's instructions. Bit1 CDD proteins migrated as major bands at 13 kDa (CDD) and 16 kDa (RPARPAR-CDD and iRGD-CDD) in Coomassie blue–stained 4% to 20% SDS-PAGE. The protein identities were confirmed by immunoblotting using antibodies against his-tag or myc-tag (Supplementary Fig. S1B). Labeled recombinant proteins were prepared by conjugating with a Dylight 550 NHS ester dye (Dy550; Pierce Biotechnology) at amine groups. The labeled protein was dialyzed and filtered (0.22 μm). Absorbance measurement was used to determine the dye concentration and degree of labeling, which was somewhat less than an average of 1 dye group per protein molecule.

Cell internalization of the recombinant proteins

Subconfluent tumor cells on chamber slides (Nalge Nunc International) were incubated with 3 μmol/L Dy550-labeled protein between 30 minutes and 24 hours. The cells were then washed 3 times with PBS and fixed with ice-cold methanol for 10 minutes. The specimens were mounted with 4′,6-diamidino-2-phenylindole (DAPI)-containing Vectashield media (Vector Laboratories) and analyzed under a confocal microscope, Olympus Fluoview 500.

Peptide-conjugated dextran was used to inhibit peptide-CDD protein for cell internalization. A thiol-reactive dextran conjugate was prepared by modifying amino-dextran 10 kDa (5.1 amines per strand, Invitrogen Life Technologies) with N-succinimidyl 3-(2-pyridyldithio)-propionate (SPDP), and dialyzed using Slide-A-Lyzer Dialysis Cassettes 3,500 molecular weight cut off (Pierce Biotechnology). To the SPDP-dextran, an excess Cys-peptide was added, followed by extensive dialysis. Each dextran molecule contained, on average, 5 copies of peptide. Inhibition assays were carried out by incubating 3 μmol/L dextran-conjugated peptide and 3 μmol/L Dy550-labeled CDD protein with PPC1 cells for 1 hour at 37°C. The cells were then washed, fixed, and analyzed by confocal microscopy as described earlier.

Published OnlineFirst December 17, 2012; DOI: 10.1158/0008-5472.CAN-12-1979

Tumor tissue penetration *ex vivo* and *in vivo*

Protein penetration in tumors was studied *ex vivo* using fresh explants of MCF-10CA1a tumors. Excised tumors were cut into pieces and incubated at 37°C with 20 μmol/L Dy550-labeled proteins in DMEM containing 1% bovine serum albumin. Binding and entry of proteins to the cut surface were examined by confocal microscopy (Olympus Fluoview 500). *In vivo* protein penetration was analyzed using orthotopic MCF-10CA1a tumor xenografts in mice. Dy550-labeled protein (20 μL of 35 μmol/L solution; approximately 10 μg protein per tumor) was injected into the center of tumor (60–80 mm^3) with spheroic shape using 31-gauge needle, and 4 hours later, entire tumors were dissected and fixed in 4% paraformaldehyde. Five-μm serial sections from entire tumors were stained with DAPI and scanned using ScanScope FL 6114 (Aperio Technologies, Inc).

Tumor treatment

Tumor-bearing mice were assigned to 3 treatment groups approximately 4 weeks after the inoculation of MCF-10CA1a cells and 9 days after the inoculation of 4T1 cells. The assignment was based on tumor size to ensure there was no statistically significant difference in tumor volume among the groups at the time the treatment began. Tumor volume was calculated from 2 diameter measurements using a digital vernier caliper and the formula: tumor volume = (length × $width^2$)/2. Proteins were diluted in PBS at 0.3 μg/μL and injected intratumorally. The injected volume was one third of the tumor volume (0.33 μL of solution per mm^3 of the tumor; ref. 12). The tip of the needle was advanced to the center of the tumor and the protein solution was injected over the course of 30 seconds. The injections were given every 3 days (a total of 4 injections in the MCF-10CA1a and 3 in the 4T1 model).

Statistical analysis

Data were analyzed by Student *t* test, one-way ANOVA, and two-way ANOVA followed by a suitable *post hoc* test using GraphPad Prism 5 software (Graphy Pad Software).

Results

Localization of Bit 1 cell death domain

Forced expression in the cytoplasm of full-length Bit1 has been shown to induce caspase-independent cell death, whereas the C-terminal catalytic domain lacks this activity (2). Hence, we focused our analysis on the N-terminal domain. To identify the CDD, we expressed a panel of N-terminally myc-tagged Bit1 fragments in HEK 293T cells, because the N-terminal tag prevents mitochondrial localization of Bit1 (2). Transient transfection of full-length Bit1 and the N-terminal 1 to 62 amino acids (F1-62) caused significant cell death, whereas various shorter fragments from the N-terminal domain showed lesser or no activity (Fig. 1 and Supplementary Fig. S2A). The catalytic Pth2 domain did not induce cell death, but instead caused a modest increase in cell viability, providing a possible explanation for the higher activity of F1-62 than full-length Bit1 (Fig. 1). The vector control had no effect on cell viability. On the basis of these results, we defined the F1-62 fragment as a Bit1 CDD.

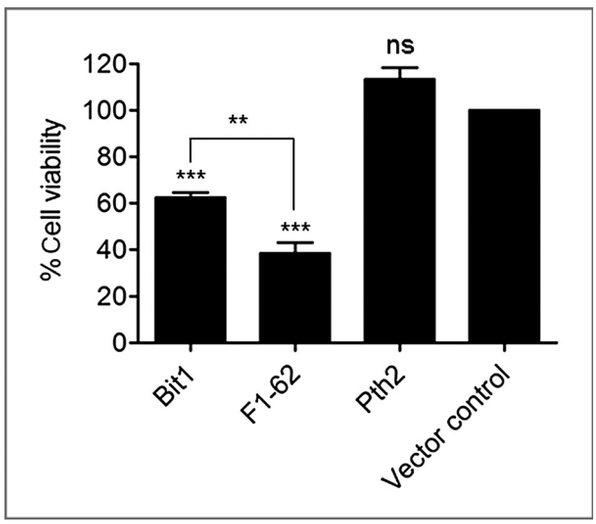

Figure 1. N-terminal fragment of Bit1 causes cell death. HEK 293T cells were transiently transfected with N-terminally myc-tagged Bit1, its N-terminal fragment F1-62, and C-terminal fragment Pth2 using FuGENE6 Transfection Reagent according to the manufacturer's instruction. The vector without Bit1 fragment served as a control. The percentage of cell viability was determined 24 hours posttransfection by MTT assay and normalized to vector control. Error bars denote mean ± SEM of 3 separate experiments carried out in triplicate of each Bit1 fragment indicated. One-way ANOVA and Student *t* test were used for statistical analysis. The comparison shown is to the vector control, or between Bit1 and F1-62. **, $P < 0.01$; ***, $P < 0.001$; ns, not significant.

The Bit1 CDD includes a conserved transmembrane segment at residues 14 to 33 (PSTLGLAVGVACGMCLGWSL) in the human Bit1 sequence (Supplementary Fig. S2B). Deleting these residues (Δ14–33) resulted in cytosolic and nuclear expression, whereas the first 13 residues were not required for the mitochondrial localization (Supplementary Fig. S2C). These findings are consistent with the enzymatic Pth2 domain exposed to the cytoplasm (Supplementary Fig. S2D and S2E).

Internalization of CendR-modified Bit1 CDD protein into cells

To deliver Bit1 CDD into cells and potentially into their cytoplasm, we fused CDD to a tumor-penetrating peptide iRGD. For comparison, we also used RPARPAR, a peptide in which the CendR motif is constitutively active. Bit1 CDD with no CendR peptide showed negligible binding to PPC1 cells, a cell line that expresses high levels of NRP-1 (Fig. 2A, a). In contrast, both RPARPAR-CDD and iRGD-CDD effectively bound to and were taken up into these cells (Fig. 2A, b and c). CDD and RPARPAR-CDD did not bind to or internalize into the NRP-1–deficient M21 cells (ref. 11; Fig 2A, d and e). iRGD-CDD bound to the surface of the M21 cells but was only weakly internalized (Fig. 2A, e), consistent with M21 cells expressing high levels of the relevant integrins (13). Cell entry of RPARPAR-CDD was rapid; after 30-minute incubation, the protein was detectable in PPC1 cells, colocalizing with NRP-1 (Fig. 2B). The amount of internalized RPARPAR-CDD peaked around 3 hours and much of the protein was found in perinuclear vesicles. Consistent with the 3-step cell entry process, internalization of iRGD-CDD was slower than

Published OnlineFirst December 17, 2012; DOI: 10.1158/0008-5472.CAN-12-1979

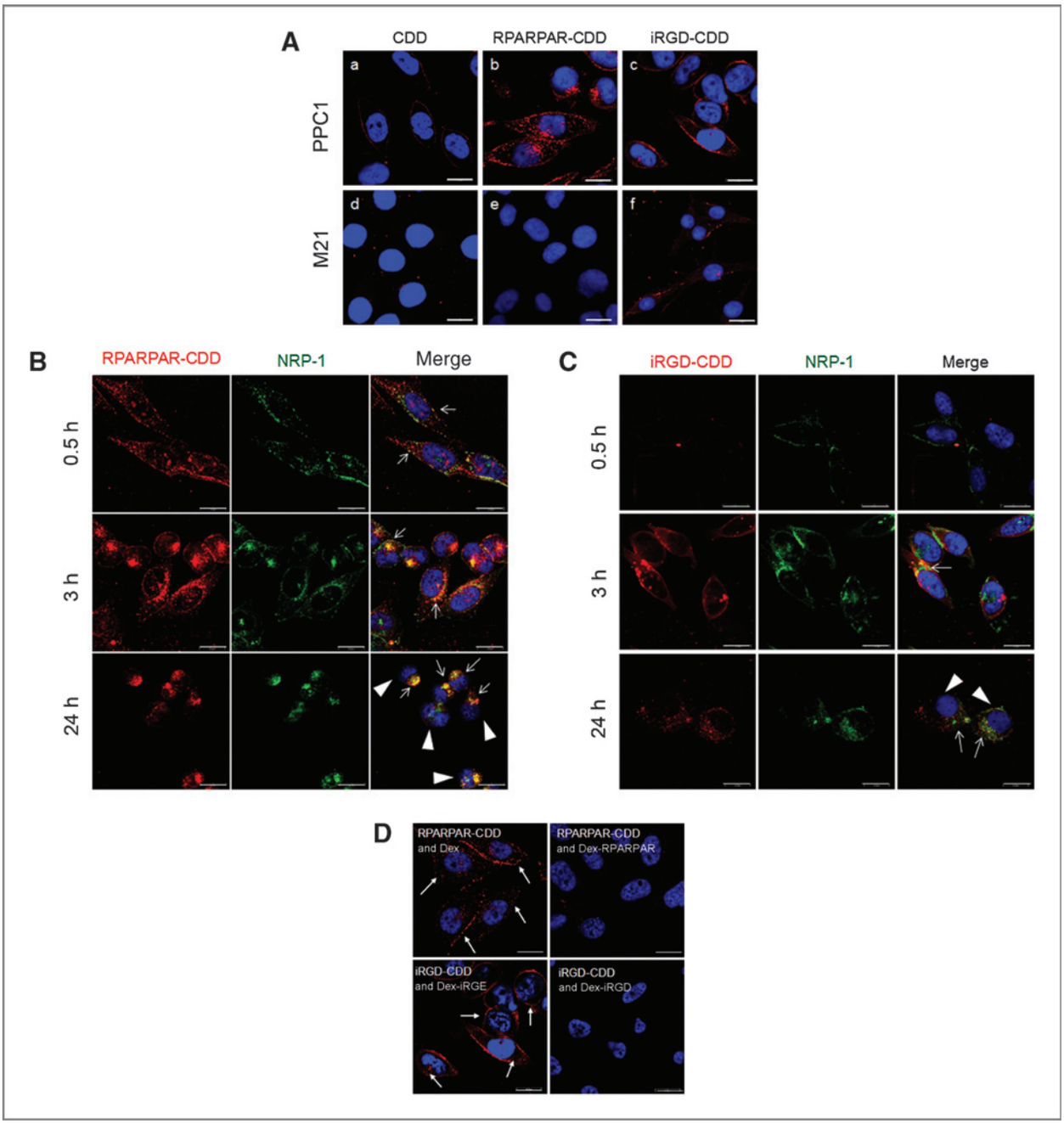

Figure 2. Internalization of CDD fusion proteins into cells. A, the PPC1 cells, which are positive for NRP-1 and αvβ3 integrin, and the NRP-1–deficient, αvβ3-positive M21 cells were incubated with 3 μmol/L fusion proteins that had been labeled with the red fluorophor Dy550. The cells were washed 3 times with PBS and fixed with cold methanol for 10 minutes. Cell nuclei were stained with DAPI (blue). The proteins were visualized by confocal microscopy (red). B and C, comparison of the localization of RPARPAR-CDD (B), and iRGD-CDD (C) with NRP-1 in PPC1 cells at various points of time. After incubation with the Dy550-labeled proteins, the cells were immunostained with an anti-NRP-1 antibody (green). Arrows indicate colocalization of the red CDD proteins and green NRP-1. The arrowheads point at cells with dying cell morphology at the 24-hour time point. D, specific inhibition of peptide-CDD fusion protein uptake into PPC1 cells by dextran (Dex)-conjugated peptides. The fusion proteins were incubated with the cells for 1 hour at 37°C in the presence of the cognate peptide inhibitors and controls. Unmodified dextran (Dex; top left) and dextran coated with iRGE (Dex-iRGE; bottom left) served as controls. Arrows point at bound and internalized RPARPAR-CDD or iRGD-CDD (red). Scale bar, 20 μm for all images.

that of RPARPAR-CDD (Fig. 2C). Twenty-four hours after these proteins were introduced into the cultures, the cells rounded up, shrank, and partially detached, indicating cell death (Fig. 2B and C). Dextran-conjugated RPARPAR and iRGD inhibited the internalization of RPARPAR-CDD and iRGD-CDD protein, respectively, whereas dextran alone or dextran conjugated with iRGE

Published OnlineFirst December 17, 2012; DOI: 10.1158/0008-5472.CAN-12-1979

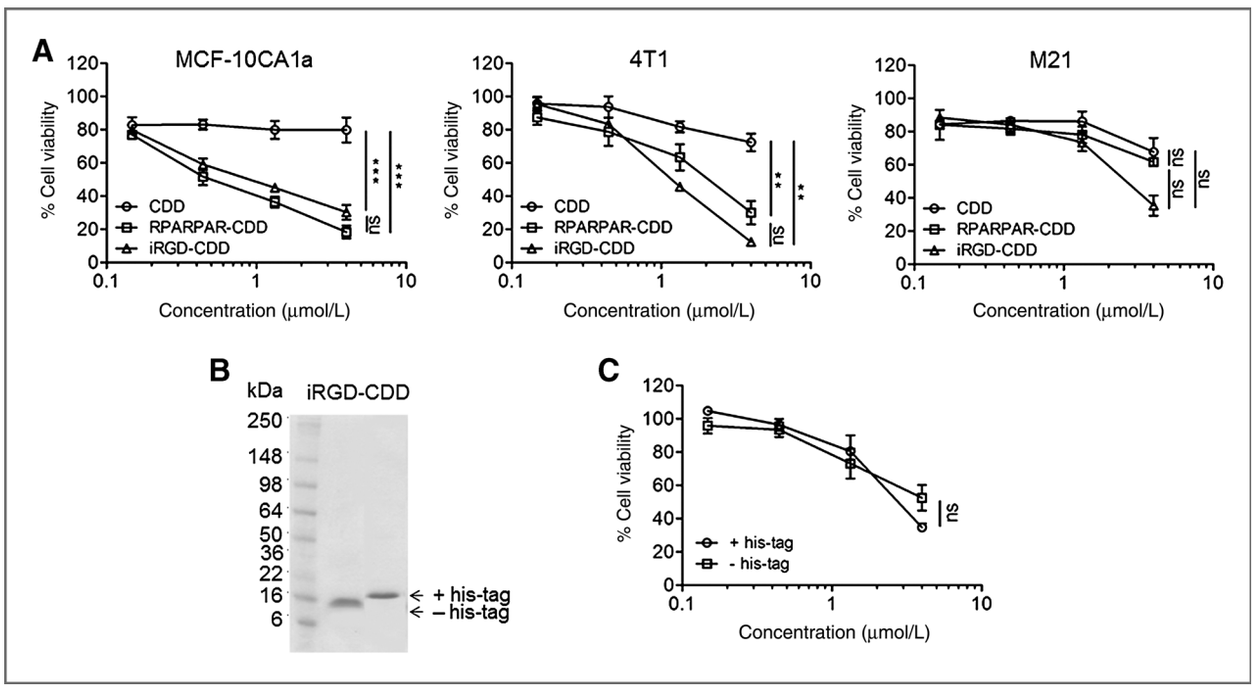

Figure 3. Cytotoxicity of CDD proteins in tumor cell lines. A, MCF-10CA1a, 4T1, and M21 cells were incubated for 48 hours with the recombinant CDD proteins at various concentrations and cell viability was measured by MTT assay. B, iRGD-CDD proteins with or without hexahistidine tag were separated on a gradient SDS-PAGE gel and visualized using Coomassie blue staining. C, MCF-10CA1a cells were incubated for 48 hours with the iRGD-CDD protein with or without a his-tag. Error bars denote mean ± SEM of 3 separate experiments carried out in quadruplicate at each concentration of the proteins. Two-way ANOVA was applied for statistical analysis. **, $P < 0.01$; ***, $P < 0.001$; ns, not significant.

(CRGEKGPDC), which does not bind to integrins showed no inhibition of the iRGD-CDD interaction with cells (Fig. 2D). These controls clearly establish the specificity of the CendR peptide-modified CDDs.

Reduction of cell viability by CendR-modified CDD proteins

Treatment of cultured breast cancer cells MCF-10CA1a and 4T1 with iRGD-CDD or RPARPAR-CDD significantly reduced cell viability, whereas nonmodified CDD protein had a modest effect at the highest concentrations or no effect at all (Fig. 3A). RPARPAR-CDD was no more cytotoxic to NRP-1–deficient M21 cells than unmodified CDD protein at the highest concentration used (3 μmol/L), indicating that the marginal toxicity at this concentration was not related to the CendR targeting. iRGD-CDD decreased M21 cell viability more than the other 2 CDD proteins, possibly because of integrin-mediated internalization, but the difference to RPARPAR-CDD and CDD was not statistically significant (Fig. 3A). These results show that the expression NRP-1, in addition to αv integrins, is needed for the effect of full cytotoxic effect of iRGD-CDD. Because cells in normal tissues do not express αv integrins, and express lower levels of NRP-1 than most tumors (14), iRGD-CDD is expected to selectively accumulate in tumors *in vivo*.

Histidine has been shown to enhance endosomal escape, explained in part by a cationic transition at low pH (15–18). Enterokinase cleaves fusion proteins containing the $(Asp)_4$-Lys recognition sequence (19), which is positioned in our construct between the his-tag and the CDD domain. The his-tag in iRGD-CDD was cleaved and removed using enterokinase and nickel-nitrilotriacetic acid affinity chromatography purification. The removal of the his-tag in the resulting iRGD-CDD was confirmed by SDS-PAGE (Fig. 3B). Cytotoxicity tests in MCF-10CA1a cells showed that the his-tag effect on construct toxicity was not significant (Fig. 3C). Thus, the his-tag plays only a minor role, if any, in the endosomal escape of the iRGD-CDD protein.

Penetration of iRGD-CDD into tumor tissue

The iRGD peptide extravasates and penetrates into extravascular tumor tissue when intravenously injected into tumor-bearing mice (10). We analyzed the penetration ability of the CDD proteins by using fresh MCF-10CA1a tumor explants. CDD showed modest binding to the cut surface of tumor tissue. iRGD-CDD, however, bound strongly and even penetrated several cell layers into the tumor tissue (Fig. 4A).

The tumor penetration activity was also apparent when fluorescently labeled iRGD-CDD was intratumorally injected into MCF-10CA1a tumors in mice. The strong iRGD-CDD signal was detectable in all sections from an entire tumor (Fig. 4B). It exhibited a web-like pattern resembling fibrotic stromal morphology (Fig. 4B, panel 5, inset a). Fibrosis is one of the major barriers that prevent drug distribution within tumor tissue. The ability of iRGD to penetrate fibrotic areas in tumors should help overcome this issue and improve local chemotherapy. The wide positive areas along the tumor periphery were presumably caused by outside-in penetration of iRGD-CDD that overflowed during the injection and the signals were not detectable outside of tumor rim (Fig. 4B,

Published OnlineFirst December 17, 2012; DOI: 10.1158/0008-5472.CAN-12-1979

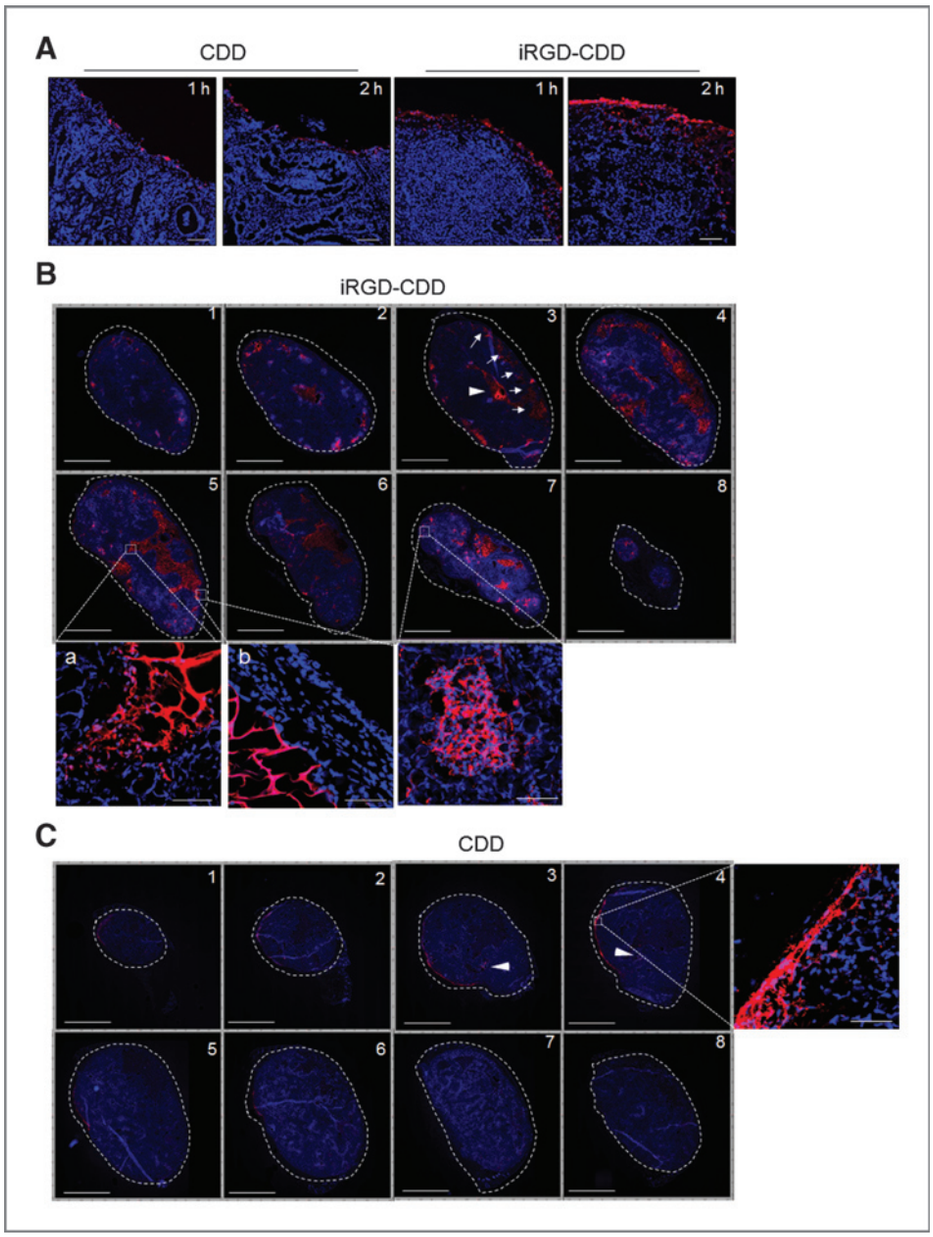

Figure 4. Tumor penetration of iRGD-CDD protein. A, penetration into tumor explants. Confocal microscopic view of MCF-10CA1a tumor explants incubated with Dy550-labeled proteins (red). Cell nuclei were stained with DAPI (blue). Scale bar, 100 μm. B and C, penetration through tumor tissue *in vivo*. Scanscopic images of serial sections from MCF-10CA1a tumors injected intratumorally with iRGD-CDD (B) or CDD (C) for 4 hours before harvesting of the tumor. The space between adjacent sections is 400 μm. Thus, the thickness from section 1 through 8 is approximately 3 mm. Tumor rims are surrounded by dotted lines. B, iRGD-CDD is abundant within the tumor, particularly in areas that appear rich in fibrotic stromal tissue (panel 5, insets a and b), as well as localized signal in parenchymal area (panel 7, inset). No signal was seen outside of tumor rim (panel 5, inset b). Arrowhead points to injection site; arrows point to the areas that presumably caused outside-in penetration of overflowed iRGD-CDD during the injection. C, the only significant signal of CDD within the tumor tissue is around the injection site (panels 3 and 4, arrowheads). Primarily CDD is located in the tumor rim (panels 3–8). Scale bar in 1 to 8, 2 mm and in the insets, 50 μm.

panel 5, inset b). Sporadic localized iRGD-CDD signals were detectable throughout the tumor suggesting protein penetration by active transport (Fig. 4B, panel 7, inset). When CDD was injected, significant intratumoral signals were only present near the injection site (Fig. 4C, panels 3 and 4). The CDD protein that overflowed during the injection remained outside the tumor rim (Fig. 4C, panels 1–6, and inset), and showed minimal penetration into the tumor tissue (Fig. 4C). The total signal of the CDD protein was lower than that of the iRGD-CDD, possibly because there is no ligand for CDD protein on tumor cells, allowing the protein to be exported from the tumor. These data support the notion that iRGD mediates active tumor penetration of the CDD protein using the NRP-1–dependent CendR pathway.

Inhibitory effect of iRGD-CDD on tumor growth in mice

Two aggressive breast tumor models MCFA-10CA1a and 4T1 were used for evaluation of antitumor effect by the iRGD-CDD protein. Etoposide, a topoisomerase inhibitor that induces caspase-dependent apoptosis in cancer cells (20), was capable of activating caspase-3 in 4T1 cells but failed in MCF-10CA1a cells, suggesting an impaired caspase cascade signaling in the MCF-10CA1a cells (Supplementary Fig. S3). This lack of correlation between CDD activity and caspase independence agrees with the previously documented caspase independence of cell death induced by the full length of Bit1 protein.

We next sought to determine whether tumor-targeted Bit1 CDD could be used as a therapeutic agent. We initially

Published OnlineFirst December 17, 2012; DOI: 10.1158/0008-5472.CAN-12-1979

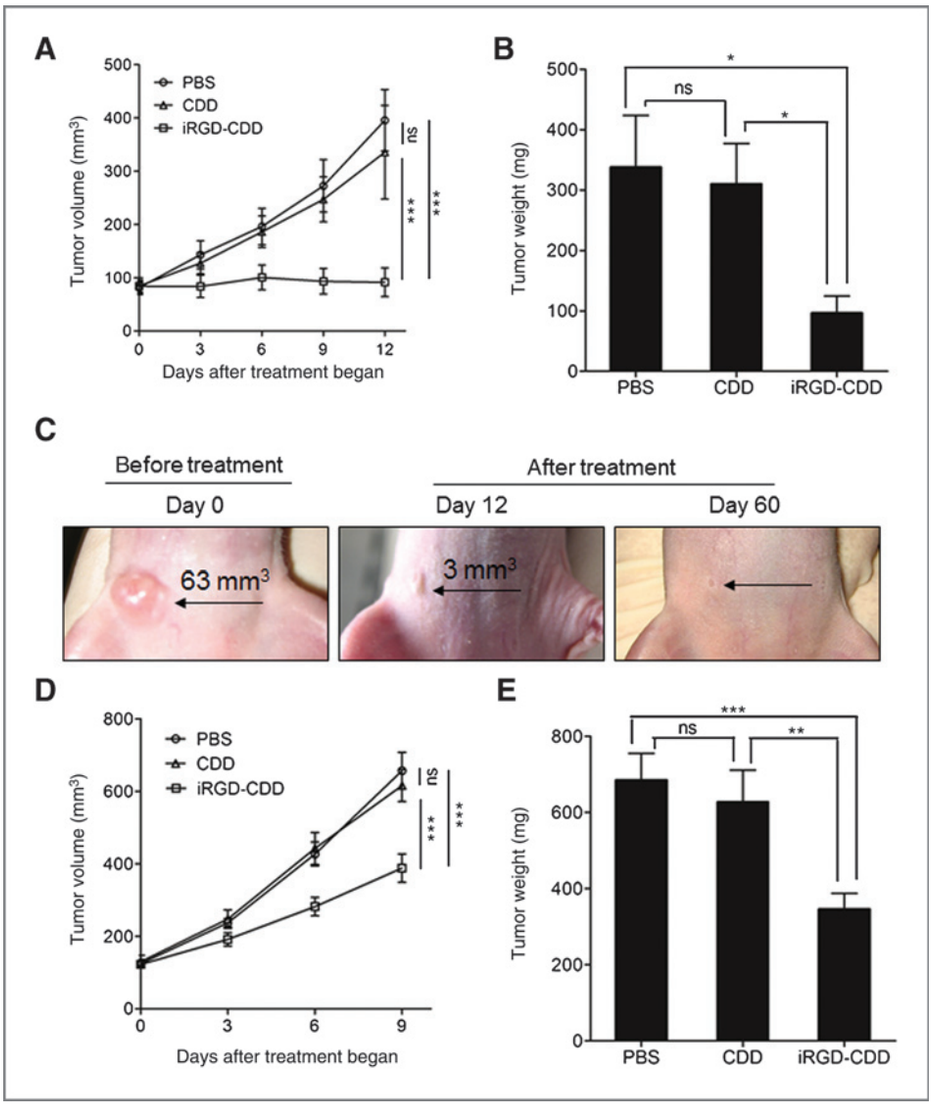

Figure 5. iRGD-CDD inhibits tumor growth in mice. Mice bearing orthotopic MCF-10CA1a (A and B; $n = 8$ mice per treatment group) or 4T1 tumors (D and E; $n = 12$ per group) were treated by intratumoral injections of PBS, CDD, or iRGD-CDD every third day. The mean tumor volume ± SEM and mean tumor weight ± SEM were plotted. Two-way ANOVA was used for the analysis of tumor volume and one-way ANOVA for the tumor weight. *, $P \leq 0.05$; **, $P \leq 0.01$; ***, $P \leq 0.001$; ns, not significant. C, eradication of tumor by intratumoral injection of iRGD-CDD. MCF-10CA1a tumor xenograft at 63 mm^3 was injected locally with iRGD-CDD every 3 days for 4 times. By the end of the treatment on day 12, tumor volume was reduced to 3 mm^3. The nodule disappeared in the following several weeks with no more treatment. Skin appeared normal around injection site during and after the treatment.

administered iRGD-CDD or CDD intravenously at 10 mg/kg of mouse body weight every other day. The initial results suggested an antitumor effect by iRGD-CDD that was not seen with CDD, but symptom of the severe toxicity required euthanasia intervention (Supplementary Fig. S4). Thus, we turned our attention to local treatment. The MCF-10CA1a tumors grew rapidly in mice treated with intratumoral injections of the PBS or CDD. In the iRGD-CDD treated mice, inhibition of tumor growth was evident as early as 3 days after the treatment began. At the end of treatment on day 12, the tumor volume was reduced by about 77% compared with the PBS and CDD controls (Fig. 5A). Tumor weights at the end of the experiments were in agreement with the size measurements; the mean weight of the tumors in the iRGD-CDD group was 30% of that in the control groups (Fig. 5B). None of the mice locally treated with iRGD-CDD or CDD alone showed any body weight loss. Notably, 2 of 8 mice (25%) in the iRGD-CDD–treated group had too small tumors to be excised after 12 days of treatment. The small nodules at the tumor inoculation site in these 2 mice disappeared during the following several weeks without any further treatment. No skin abnormalities were observed around the injection sites, suggesting the tumor-specific penetration of iRGD-CDD (Fig. 5C). The mice were healthy and had no signs of tumor metastasis during 6 months of observation.

The treatment results in the 4T1 tumor model were also positive but reflected the greater aggressiveness of these tumors than the MCF-10CA1a tumors. Tumor volume in iRGD-CDD group was about 40% and tumor weight about 50% smaller than in the PBS and CDD control groups (Fig. 5D and E).

Hematoxylin and eosin (H&E)–stained tumor sections did not show differences among tumors treated with iRGD-CDD, CDD, or PBS (Fig. 6A). Tumors from the iRGD-CDD groups, however, showed significantly stronger TUNEL staining than tumors treated with PBS or CDD, indicating substantial cell death in the iRGD-CDD–treated tumors (Fig. 6B). In agreement

Published OnlineFirst December 17, 2012; DOI: 10.1158/0008-5472.CAN-12-1979

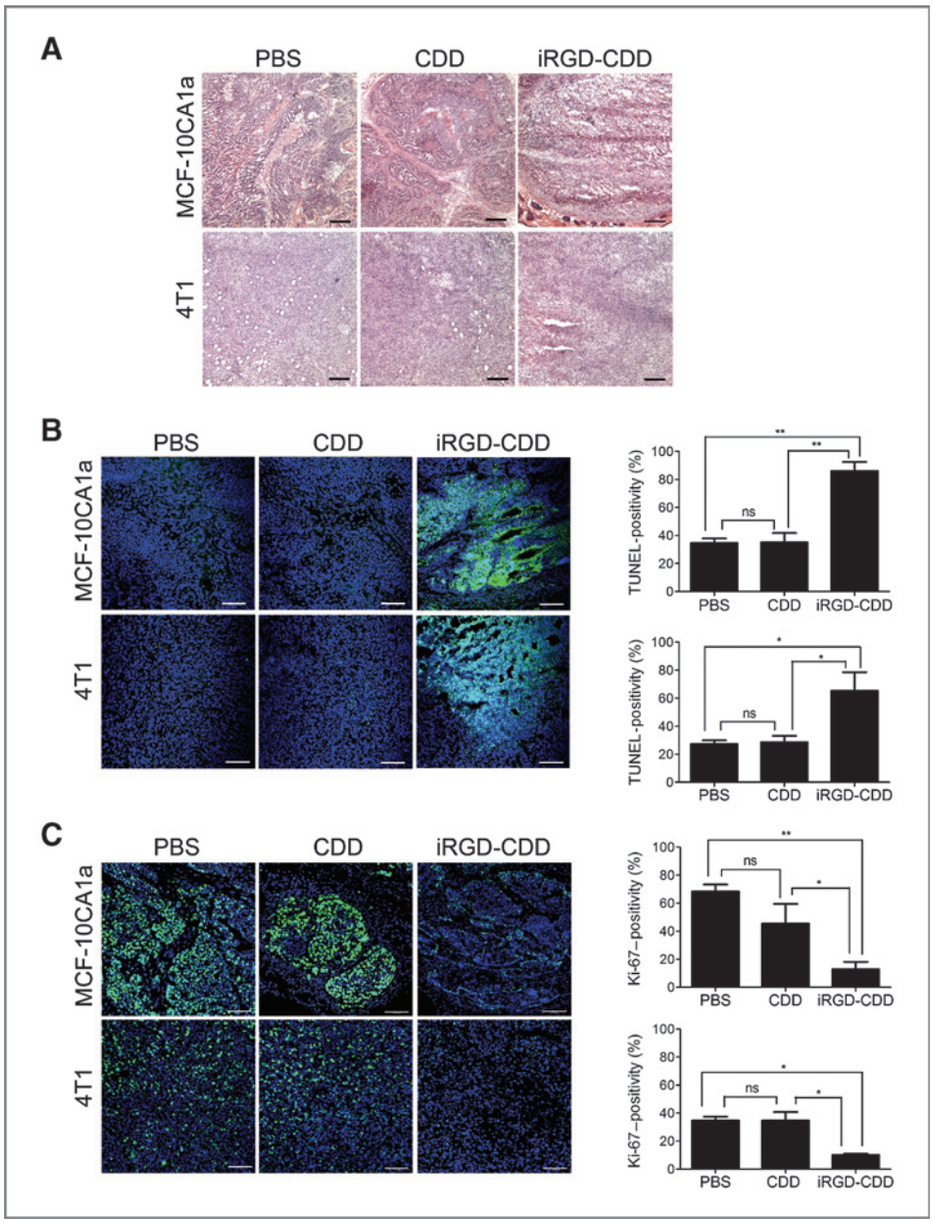

Figure 6. Analysis for cell death and antiproliferative effect of iRGD-CDD in tumors. A, H&E staining of tumor sections from mice treated with intratumoral injections of PBS, CDD, or iRGD-CDD. B, cell death was analyzed by TUNEL staining (green). Nuclei were stained with DAPI (blue). TUNEL-positivity was quantified by normalizing TUNEL signal to DAPI (right). C, cell proliferation was analyzed by immunostaining of tumor sections using a rabbit anti-Ki-67 polyclonal antibody, followed by Alex Flour-488 conjugated anti-rabbit IgG (green). Nuclei were stained with DAPI (blue). Ki-67 expression was quantified by normalizing the Ki-67 signal to DAPI signal (right). Error bars denote mean $\pm$ SEM. *, $P \leq 0.05$; **, $P \leq 0.01$; ns, not significant. Scale bar, 100 μm for all images.

with the TUNEL result, staining for the Ki-67 marker of cell proliferation was significantly lower in the iRGD-CDD–treated tumors than in the PBS or CDD controls (Fig. 6C).

Discussion

In this work, we define the Bit1 CDD, localize it to the presumed membrane-embedded domain of the protein and show that CDD is more potent than full-length Bit1 in causing cell death when tested by cDNA transfection. We also show that the CDD protein is highly active when introduced into tumor cells using protein transduction mediated by the tumor-penetrating and cell-internalizing peptide iRGD, and that the fusion protein is a promising antitumor agent capable of spreading within tumor tissue from an intratumoral injection.

Our results place the CDD of Bit1 in the N-terminal domain, which contains the 20-amino acid hydrophobic sequence thought to anchor Bit1 to the mitochondrial outer membrane. Targeting of polypeptides encoded in the nucleus to mitochondria requires the presence of a signal sequence for mitochondrial localization. Most of these sequences contain positively charged amphipathic α-helical stretch at the N-terminus, followed by a stretch of hydrophobic residues (21). The Bit1 N-terminus fulfills these criteria (Supplementary Fig. S2A). The mitochondrial signal sequences can direct a protein through both of the mitochondrial membranes to the interior of mitochondria, to the space between the outer and inner membranes, or anchor a protein to the outer membrane (22–24). Our results show that Bit1 is available for protease

Published OnlineFirst December 17, 2012; DOI: 10.1158/0008-5472.CAN-12-1979

digestion at the surface of intact mitochondria (Supplementary Fig. S2D). Thus, Bit1 membrane-embedded domain likely attaches the protein to the outer mitochondrial membrane without mediating transfer through the membrane.

Recent results provide clues to the mechanisms underlying Bit1 and Bit1 CDD-mediated cell death. Bit 1, when translocated to the cytoplasm from the mitochondria, interacts with the Groucho/TLE family member AES, suggesting that Bit1 may regulate the activities of the antiapoptotic and oncogenic TLE proteins (2, 6, 25). Other results show that disrupting Bit1 expression with short hairpin RNA confers weakly malignant MCF7 cells enhanced anoikis resistance and increased migratory potential. These changes correlated with an increase in active Erk levels and a decrease in Erk-directed phosphatase activity (26), providing another possible mechanism for the reduced viability of cells with increased Bit1 activity.

We showed the CDD activity and specificity using 2 methods, cDNA transfection and protein transduction. As CDD is thought to act in the cytoplasm and the effects of the protein transduction and cDNA transfection were similar, we infer that the CendR peptides delivered CDD into the cytoplasm. This is the first demonstration that peptides using the CendR pathway can be active in protein transduction.

Traditional cell-penetrating peptides have been used to deliver recombinant proteins to mammalian cells (27, 28), but these peptides are nonselective; they promote entry into all cells. The prototype of these peptides, Tat, resembles our peptides in that it contains several CendR (R/KXXR/K) motifs (11). However, Tat is active whether fused to the N- or C-terminus of a protein, whereas the activity of CendR peptides is position-dependent in that the CendR motif must be exposed at the C-terminus to be active (11). Hence, activation of peptides with cryptic CendR motifs in a target tissue can be used in tissue-specific delivery of payloads. Indeed, our tumor-homing CendR peptides, such as iRGD and LyP-1 are specific for tumors, whereas the Tat-type peptides are not specific for any cell type or tissue (10, 29). Thus, the tumor-specific CendR peptides offer new opportunities for cell type–specific and tissue-specific protein transduction.

The iRGD peptide selectively activates the CendR trans-tissue transport pathway in tumor, taking payloads as large as nanoparticles with it (10, 14, 30, 31). Here, we show that these peptides can provide a protein with an anticancer activity and the ability to penetrate into tumor tissue from a local site without affecting the surrounding normal tissue.

We made use of the tumor penetration activity of iRGD-CDD in a new anticancer treatment. Treating-tumor bearing mice with iRGD-CDD effectively inhibited tumor growth *in vivo*, causing nearly 80% reduction in tumor volume of the MCF-10CA1a tumors and 40% reduction in 4T1 tumors. Importantly, 25% of the MCF-10CA1a tumors were eradicated by the iRGD-CDD treatment. Targeting caspase independency for tumor therapeutics is a promising strategy to eliminate cancer cells because tumor cells often develop resistance to antitumor agents by developing defects in caspase activation. Activating a caspase-independent cell death pathway with Bit1 CDD may be an effective way of attacking tumor cells resistant to apoptosis. Caspase activation is blocked in the MCF-10CA1a cells, whereas this pathway is intact in the 4T1 cells. The greater inhibitory effect of Bit1 CDD in the MCF-10CA1a tumor than in the 4T1 tumor suggests an inverse correlation between the activities of the caspase-dependent cell death pathways (32).

Intratumoral treatment may be particularly useful for tumors that are difficult to remove surgically or treated systemically. Advanced tumors in vital organs can be unresectable, and some tumors are protected from systemic chemotherapy by the blood–brain barrier and fibrotic stroma. Indeed, adjuvant local chemotherapy has been applied to malignant glioma and tested in advanced tumors localizing in the lungs, pancreas, and esophagus (33–37). However, poor drug spreading within the tumor tissue has been a limiting factor for successful local tumor therapies (38, 39). iRGD-CDD, the novel tumor-penetrating cell death protein, may significantly advance local tumor therapies and offer new treatment options to cancer with locally advanced tumors.

Disclosure of Potential Conflicts of Interest

K.N. Sugahara and T. Teesalu have ownership interest (including patents) in CendR Therapeutics Inc. E. Ruoslahti is the founder, chairman of the board, consultant/advisory board member, and major shareholder of CendR Therapeutics Inc. and has ownership interest (including patents) in the same. No potential conflicts of interest were disclosed by the other authors.

Authors' Contributions

Conception and design: R. Chen, K.N. Sugahara, T. Teesalu, E. Ruoslahti
Development of methodology: R. Chen, G.B. Braun, K.N. Sugahara, T. Teesalu
Acquisition of data (provided animals, acquired and managed patients, provided facilities, etc.): X. Luo, T. Teesalu
Analysis and interpretation of data (e.g., statistical analysis, biostatistics, computational analysis): R. Chen, G.B. Braun, X. Luo, K.N. Sugahara, T. Teesalu, E. Ruoslahti
Writing, review, and/or revision of the manuscript: R. Chen, G.B. Braun, K. N. Sugahara, T. Teesalu, E. Ruoslahti
Administrative, technical, or material support (i.e., reporting or organizing data, constructing databases): R. Chen, E. Ruoslahti
Study supervision: K.N. Sugahara, E. Ruoslahti

Acknowledgments

The authors thank Dr. Eva Engvall for comments on the article, Christopher Brunquell for scientific discussions, and Paul Kirsch for editorial assistance.

Grant Support

This work was supported by grants W81XWH-10-1-0198 and W81XWH-08-1-0727 from the DOD (E. Ruoslahti) and Cancer Center Support Grant CA30199 from the National Cancer Institute.

The costs of publication of this article were defrayed in part by the payment of page charges. This article must therefore be hereby marked *advertisement* in accordance with 18 U.S.C. Section 1734 solely to indicate this fact.

Received May 22, 2012; revised October 19, 2012; accepted November 5, 2012; published OnlineFirst December 17, 2012.

References

1. Frisch SM, Vuori K, Ruoslahti E, Chan-Hui PY. Control of adhesion-dependent cell survival by focal adhesion kinase. J Cell Biol 1996;134:793–9.

2. Jan Y, Matter M, Pai JT, Chen YL, Pilch J, Komatsu M, et al. A mitochondrial protein, Bit1, mediates apoptosis regulated by integrins and Groucho/TLE corepressors. Cell 2004;116:751–62.

Published OnlineFirst December 17, 2012; DOI: 10.1158/0008-5472.CAN-12-1979

3. Biliran H, Jan Y, Chen R, Pasquale EB, Ruoslahti E. Protein kinase D is a positive regulator of Bit1 apoptotic function. J Biol Chem 2008;283:28029–37.
4. Kairouz-Wahbe R, Biliran H, Luo X, Khor I, Wankell M, Besch-Williford C, et al. Anoikis effector Bit1 negatively regulates Erk activity. Proc Natl Acad Sci U S A 2008;105:1528–32.
5. Matsuyama A, Hisaoka M, Iwasaki M, Iwashita M, Hisanaga S, Hashimoto H. TLE1 expression in malignant mesothelioma. Virchows Arch 2010;457:577–83.
6. Sonderegger CK, Vogt PK. Binding of the corepressor TLE1 to Qin enhances Qin-mediated transformation of chicken embryo fibroblasts. Oncogene 2003;22:1749–57.
7. De Pereda JM, Waas WF, Jan Y, Ruoslahti E, Schimmel P, Pascual J. Crystal structure of a human peptidyl-tRNA hydrolase reveals a new fold and suggests basis for a bifunctional activity. J Biol Chem 2004;279:8111–5.
8. Hambley TW, Hait WN. Is anticancer drug development heading in the right direction? Cancer Res 2009;69:1259–62.
9. Minchinton AI, Tannock IF. Drug penetration in solid tumours. Nat Rev Cancer 2006;6:583–92.
10. Sugahara KN, Teesalu T, Karmali PP, Kotamraju VR, Agemy L, Girard OM, et al. Tissue-penetrating delivery of compounds and nanoparticles into tumors. Cancer Cell 2009;16:510–20.
11. Teesalu T, Sugahara KN, Kotamraju VR, Ruoslahti E. C-end rule peptides mediate neuropilin-1-dependent cell, vascular, and tissue penetration. Proc Natl Acad Sci U S A 2009;106:16157–62.
12. Giustini AJ, Ivkov R, Hoopes PJ. Magnetic nanoparticle biodistribution following intratumoral administration. Nanotechnology 2011;22:345101.
13. Cheresh DA, Spiro RC. Biosynthetic and functional properties of an Arg–Gly–Asp–directed receptor involved in human melanoma cell attachment to vitronectin, fibrinogen, and von Willebrand factor. J Biol Chem 1987;262:17703–11.
14. Ruoslahti E. Peptides as targeting elements and tissue penetration devices for nanoparticles. Adv Mater 2012;24:3747–56.
15. Chang KL, Higuchi Y, Kawakami S, Yamashita F, Hashida M. Efficient gene transfection by histidine-modified chitosan through enhancement of endosomal escape. Bioconjug Chem 2010;21:1087–95.
16. Hatefi A, Megeed Z, Ghandehari H. Recombinant polymer-protein fusion: a promising approach towards efficient and targeted gene delivery. J Gene Med 2006;8:468–76.
17. Lo SL, Wang S. An endosomolytic Tat peptide produced by incorporation of histidine and cysteine residues as a nonviral vector for DNA transfection. Biomaterials 2008;29:2408–14.
18. Stevenson M, Ramos-Perez V, Singh S, Soliman M, Preece JA, Briggs SS, et al. Delivery of siRNA mediated by histidine-containing reducible polycations. J Control Release 2008;130:46–56.
19. Collins-Racie LA, McColgan JM, Grant KL, DiBlasio-Smith EA, McCoy JM, LaVallie ER. Production of recombinant bovine enterokinase catalytic subunit in Escherichia coli using the novel secretory fusion partner DsbA. Biotechnology (N Y) 1995;13:982–7.
20. Kaufmann SH. Induction of endonucleolytic DNA cleavage in human acute myelogenous leukemia cells by etoposide, camptothecin, and other cytotoxic anticancer drugs: a cautionary note. Cancer Res 1989;49:5870–8.
21. Schmidt O, Pfanner N, Meisinger C. Mitochondrial protein import: from proteomics to functional mechanisms. Nat Rev Mol Cell Biol 2010;11:655–67.
22. Rapaport D. Finding the right organelle. Targeting signals in mitochondrial outer-membrane proteins. EMBO Rep 2003;4:948–52.
23. van der Laan M, Hutu DP, Rehling P. On the mechanism of preprotein import by the mitochondrial presequence translocase. Biochim Biophys Acta 2010;1803:732–9.
24. Waizenegger T, Stan T, Neupert W, Rapaport D. Signal-anchor domains of proteins of the outer membrane of mitochondria: structural and functional characteristics. J Biol Chem 2003;278:42064–71.
25. Zhang X, Chen HM, Jaramillo E, Wang L, D'Mello SR. Histone deacetylase-related protein inhibits AES-mediated neuronal cell death by direct interaction. J Neurosci Res 2008;86:2423–31.
26. Karmali PP, Brunquell C, Tram H, Ireland SK, Ruoslahti E, Biliran H. Metastasis of tumor cells is enhanced by downregulation of Bit1. PLoS ONE 2011;6:e23840.
27. Wadia JS, Dowdy SF. Modulation of cellular function by TAT mediated transduction of full length proteins. Curr Protein Pept Sci 2003;4:97–104.
28. Zhou H, Wu S, Joo JY, Zhu S, Han DW, Lin T, et al. Generation of induced pluripotent stem cells using recombinant proteins. Cell Stem Cell 2009;4:381–4.
29. Roth L, Agemy L, Kotamraju VR, Braun G, Teesalu T, Sugahara KN, et al. Transtumoral targeting enabled by a novel neuropilin-binding peptide. Oncogene 2012;31:3754–63.
30. Ruoslahti E, Bhatia SN, Sailor MJ. Targeting of drugs and nanoparticles to tumors. J Cell Biol 2010;188:759–68.
31. Sugahara KN, Teesalu T, Karmali PP, Kotamraju VR, Agemy L, Greenwald DR, et al. Coadministration of a tumor-penetrating peptide enhances the efficacy of cancer drugs. Science 2010;328:1031–5.
32. Broker LE, Kruyt FA, Giaccone G. Cell death independent of caspases: a review. Clin Cancer Res 2005;11:3155–62.
33. Celikoglu F, Celikoglu SI, Goldberg EP. Bronchoscopic intratumoral chemotherapy of lung cancer. Lung Cancer 2008;61:1–12.
34. Elstad NL, Fowers KD. OncoGel (ReGel/paclitaxel)—clinical applications for a novel paclitaxel delivery system. Adv Drug Deliv Rev 2009;61:785–94.
35. Engelhard HH. Gene therapy for brain tumors: the fundamentals. Surg Neurol 2000;54:3–9.
36. Hecht JR, Bedford R, Abbruzzese JL, Lahoti S, Reid TR, Soetikno RM, et al. A phase I/II trial of intratumoral endoscopic ultrasound injection of ONYX-015 with intravenous gemcitabine in unresectable pancreatic carcinoma. Clin Cancer Res 2003;9:555–61.
37. Lawson HC, Sampath P, Bohan E, Park MC, Hussain N, Olivi A, et al. Interstitial chemotherapy for malignant gliomas: the Johns Hopkins experience. J Neurooncol 2007;83:61–70.
38. Boucher Y, Brekken C, Netti PA, Baxter LT, Jain RK. Intratumoral infusion of fluid: estimation of hydraulic conductivity and implications for the delivery of therapeutic agents. Br J Cancer 1998;78:1442–8.
39. Wang CC, Li J, Teo CS, Lee T. The delivery of BCNU to brain tumors. J Control Release 1999;61:21–41.

Published OnlineFirst December 17, 2012; DOI: 10.1158/0008-5472.CAN-12-1979

Cancer Research
The Journal of Cancer Research (1916–1930) | The American Journal of Cancer (1931–1940)

AACR American Association for Cancer Research

Application of a Proapoptotic Peptide to Intratumorally Spreading Cancer Therapy

Renwei Chen, Gary B. Braun, Xiuquan Luo, et al.

Cancer Res 2013;73:1352-1361. Published OnlineFirst December 17, 2012.